A FLIGHT INVESTIGATION OF STEADY-STATE AND DYNAMIC PRESSURE PHENOMENA IN THE

AIR INLETS OF SUPERSONIC AIRCRAFT

Frank W. Burcham, Jr.
Aerospace Engineer

and

Donald R. Bellman
Assistant Director of Research, Flight Mechanics

NASA Flight Research Center
P. O. Box 273
Edwards, California 93523

SUMMARY

The difficulty of achieving adequate inlet performance and stability and avoiding engine compressor stalls at supersonic speeds has led the NASA Flight Research Center to investigate the pressure phenomena in the inlets of several supersonic aircraft. Results of recent tests with the F-111A airplane are presented showing the inlet steady-state and dynamic performance. The inlet total pressure distortion that causes compressor stall is discussed, and the requirement for high response instrumentation is demonstrated. A duct resonance encountered at Mach numbers near 2.0 is analyzed and shown to be due to a normal shock oscillation at the duct fundamental frequency. Various statistical parameters are used in the analysis. Another resonance, in the engine fan duct, is shown to be a possible cause of reduced engine stall margin in afterburning operation. Plans for a comprehensive inlet study of the YF-12 airplane are discussed including flight tests and full-scale, 1/3-scale, and 1/12-scale wind-tunnel tests.

SYMBOLS

K_D	Pratt & Whitney distortion factor (see page 24-5)	α	angle of attack, deg
M	Mach number	Δ	increment
$\dfrac{m}{m_0}$	mass flow ratio, $\dfrac{w2}{w_\infty}$	δ_{t_2}	ratio of average compressor face total pressure to sea-level standard pressure
N_1	fan speed, rpm	θ_c	inlet second cone angle, deg
p	static pressure, kN/m^2		
p_t	total pressure, kN/m^2	θ_{t_2}	ratio of local total temperature to sea-level standard temperature
T_t	total temperature, °K		

Subscripts:

T_u	turbulence factor (see page 24-5)	av	average
		rms	root mean square
t	time, sec	∞	free stream
w	airflow, kg/sec	2	compressor face
$\dfrac{X}{R}$	ratio of distance, X, between inlet cowl lip and spike tip to inlet cowl radius, R, 84.56 cm	2.6	fan discharge
		3	low pressure compressor discharge
		4	high pressure compressor discharge

INTRODUCTION

Aircraft that have air-breathing propulsion systems and fly at transonic and supersonic speeds have the problem of achieving adequate inlet pressure recovery for efficient operation of the propulsion system without producing undesirable conditions such as flow distortion and fluctuations which can often lead to compressor stalls and inlet unstarts. A better understanding of these inlet conditions is needed to improve techniques for designing inlets on future aircraft. However, such complex flows are difficult to predict theoretically and to duplicate accurately in ground facilities. Therefore the NASA Flight Research Center at Edwards, California, has a continuing program to measure steady-state and dynamic conditions within jet engine inlets in full-scale flight.

This program was started on the XB-70 airplane and later extended to two F-111A airplanes. Results of the XB-70 tests are presented in references 1 and 2. Reference 1 also describes the instrumentation used in the later F-111A tests. Initial results from the F-111A flight tests are presented in reference 3, and additional data together with an analysis which conclusively shows the need for high response instrumentation in relating inlet flow distortion to the occurrence of engine compressor stall are given in reference 4.

In the first F-111A airplane, steady-state and dynamic pressure rakes were alternated at the compressor face and intermixed throughout the inlet duct. In a later series of tests on a second airplane, the dynamic and steady-state pressure measurements at the compressor face were both increased from 20 to 40 by using rakes which permitted each sensor to measure absolute pressure levels as well as dynamic fluctuations. Propulsion system data were recorded in flight maneuvers at Mach numbers up to 2.2 and at altitudes up to 15,000 meters for various power settings and inlet geometry conditions.

This paper presents results from both F-111A flight programs with emphasis on the dynamic flow conditions within the inlet and fan ducts. Plans and preparations for the extension of these propulsion system studies to another type of inlet and to a Mach number of 3 using a YF-12 airplane are also described.

DESCRIPTION OF F-111A AIRPLANE

The F-111A airplane is a current multimission tactical fighter with variable sweep wings. With the wings in the forward position, the airplane is capable of short takeoff and landing and efficient subsonic cruise. With the wings

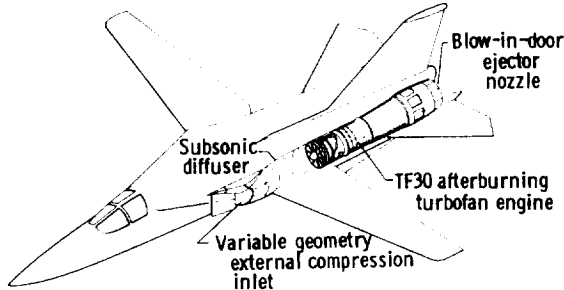Figure 1. Photograph of the two F-111A test airplanes.
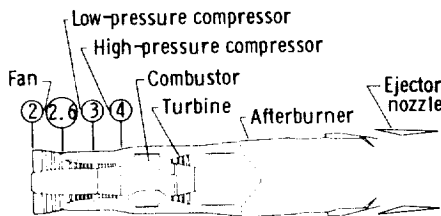

Figure 2. F-111A left propulsion system.

Figure 3. TF30 afterburning turbofan engine and appropriate station designations.

swept, the airplane is designed for supersonic dash capability at sea level and Mach 2.5 at altitude.

The two F-111A airplanes used in the NASA tests were both early models, numbers 6 and 12 (fig. 1). The only significant differences between the airplanes for these tests were in the inlet, as discussed later.

Propulsion System

The left propulsion system of the F-111A airplane is shown in figure 2. Thrust is provided by two TF30 afterburning turbofan engines mounted in the aft fuselage. The engines are equipped with blow-in-door ejector nozzles that admit external air at low speeds to control nozzle expansion. Air is supplied to the engine by an inlet mounted under the wing glove followed by a short subsonic diffuser.

Engine.— The TF30-P-1 engine has approximately 80,000 newtons of thrust and a nominal bypass ratio of 1.0. Figure 3 is a schematic view of the engine. A three-stage fan and a six-stage low pressure compressor is driven by a three-stage turbine at N_1 speed. A seven-stage high pressure compressor is driven by a separate turbine. Rated airflow is 110 kilograms per second and overall compression ratio is 17 to 1. A five-zone afterburner is located in the combined fan and core streams. The engines tested were equipped with sixth-stage bleeds to increase the distortion tolerance of the compressor. These bleeds were usually opened for Mach numbers above 1.8. The engines tested in the two airplanes were essentially identical. More information on the engine is included in references 4 and 5.

Inlet.— The air inlet shown in figures 4 and 5 is a variable-geometry external-compression type and is approximately a 90° segment of a double cone axisymmetric inlet. Inlet geometry can be varied by translating the compression spike fore and aft and by varying the second conical ramp (cone) angle from 10.5° to 24°. The first conical ramp is fixed at 12.5°.

At low speeds the spike is forward and the cone is collapsed, as shown in figure 4. At high supersonic speeds, the spike is aft and the cone is fully expanded. This configuration is shown in figure 5. Positions of the spike and cone are normally controlled by an automatic inlet control system, described in reference 6. The left inlet geometry could be manually positioned by the pilot to any desired position on both test airplanes.

Two different cowl lip configurations were tested. A sharp lip cowl (fig. 4) was tested on both airplanes. A cowl with a blunted lip (fig. 5) was flown on airplane number 6 for several flights. This cowl, in addition to the more rounded lip, was drooped and cut back 5 centimeters over the inboard part and had a slightly larger capture area.
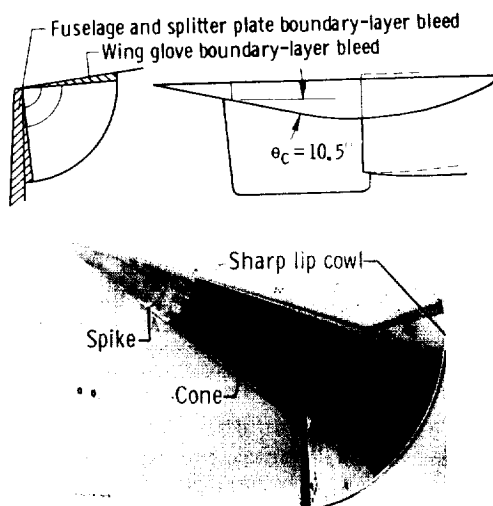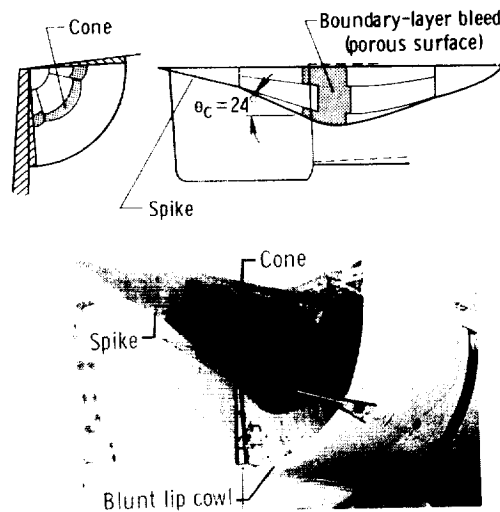

Figure 4. Photograph and two-view drawing of the F-111A inlet with sharp lip cowl installed, spike full forward, and cone fully collapsed.

Figure 5. Photograph and two-view drawing of the F-111A inlet with blunt lip cowl installed, spike full aft, and cone fully expanded.

Subsonic diffuser.— The inlet subsonic diffuser (fig. 2) turns inboard and changes in shape from a one-quarter circle near the inlet to a circular shape at the compressor face in a relatively short length. The cross-sectional area
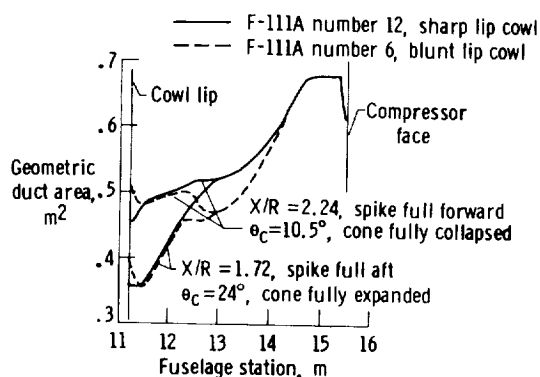
Figure 6. Inlet duct area distribution for F-111A number 6 and number 12.

distributions for both airplanes are shown in figure 6. It can be seen that the latter configuration (airplane number 12) diffuses the air more gradually in the middle part of the duct. Vortex generators (fig. 7) are installed to minimize separation in the duct and to improve the pressure distribution at the compressor face.

Boundary-layer removal system.— The F-111A inlet incorporates several regions of boundary-layer removal to prevent low energy air from entering the inlet. Fuselage, splitter plate, and wing glove bleed scoops are shown in figure 4 and porous bleed on the second cone surface in figure 5.

INSTRUMENTATION

Figure 7 shows the location of pressure measurements in the left inlet of the F-111A airplane. Table 1 describes the number of measurements, their sampling rates, and their frequency responses for the airplanes. Miniature
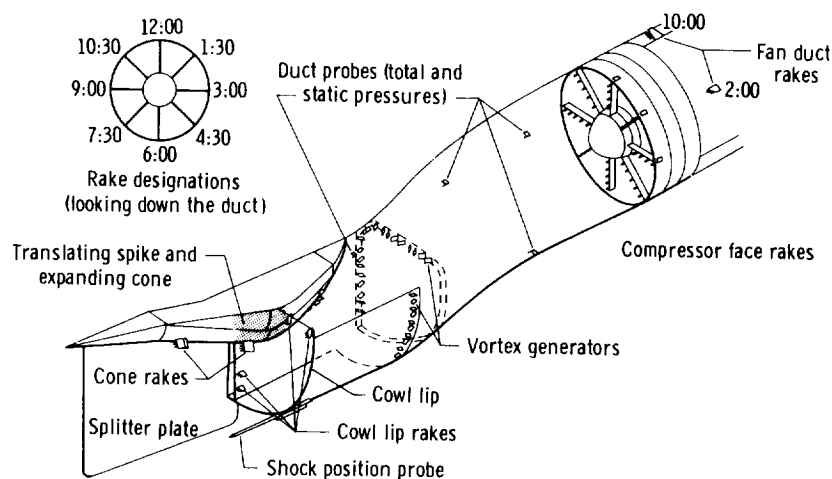

Figure 7. Inlet and compressor face pressure instrumentation.

TABLE 1.— NUMBER OF MEASUREMENTS, SAMPLING RATE, AND FREQUENCY RESPONSE OF PRESSURES IN THE F-111A INLET

Location of pressures	Number of measurements		Samples per second	Frequency response, Hz
	F-111A no. 6	F-111A no. 12		
Cone rake:				
Total pressure	8	--	400	200
Static pressure	2	--	400	200
Cowl lip:				
Total pressure	12	--	200	100*
Static pressure	4	--	200	100*
Shock position probe	6	--	200	100*
Inlet duct:				
Total pressure	4	--	200	100
Static pressure	4	--	200	100
Compressor face:				
Total pressure, low response	20	--	50	10
Total pressure, high response	20	40	400	200
Compressor face:				
Total pressure	2	2	Analog	1000
Static pressure	16	4	200	100*
Fan duct total pressure	8	--	200	100*
Low compressor discharge static pressure	1	1	200	100*
High compressor discharge static pressure	1	1	200	100*

*Parameter filtered at 40 hertz prior to digitizing; amplitude uncertain above 40 hertz.

transducers were located in the two cone rakes, the shock position probe, the duct rakes, and the diagonally oriented compressor face rakes to provide high frequency response. Conventional probes connected by tubes to remotely located transducers were used for the cowl lip rakes, the horizontal and vertically oriented compressor face rakes, and internal engine instrumentation. The tube lengths limited flat frequency response to about 50 hertz. Details of the instrumentation on airplane number 6 are included in references 1 and 3 through 6. Differential pressure transducers were used for all measurements except the internal engine measurements. Some of the techniques used to obtain the dynamic pressure measurements are described in reference 7.

The miniature transducers gave good values for dynamic pressure but were subject to large zero shifts due to temperature changes, and their steady-state values were not reliable. Eight high response compressor face rakes were flown in airplane number 12. These were a special type with in-flight nulling capability to determine the transducer zero, as often as desired, so that steady-state as well as dynamic values could be obtained. Details of the rake design are presented in reference 7. Figure 8 is a photograph showing the rake installation at the engine compressor face. A schematic view of this rake is shown in figure 9. Figure 10 shows an example of the rake zero checks made on two compressor face total pressures before and after a compressor stall.
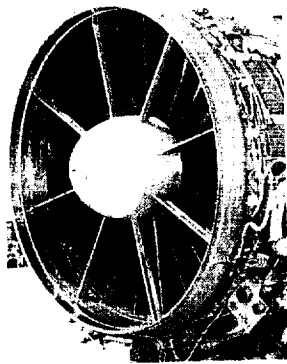
Figure 8. Photograph of the TF30 engine showing the compressor face rakes with in-flight nulling capability.
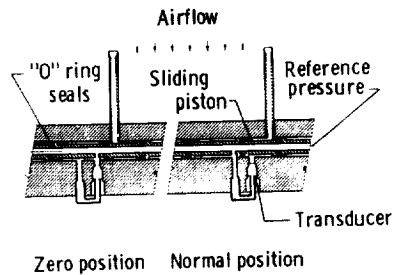

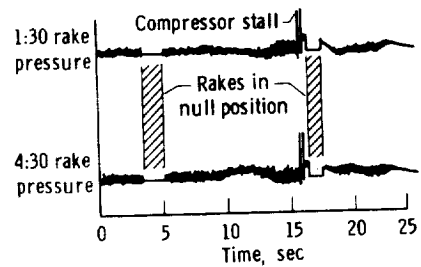Figure 9. High response compressor face rake with in-flight nulling capability.

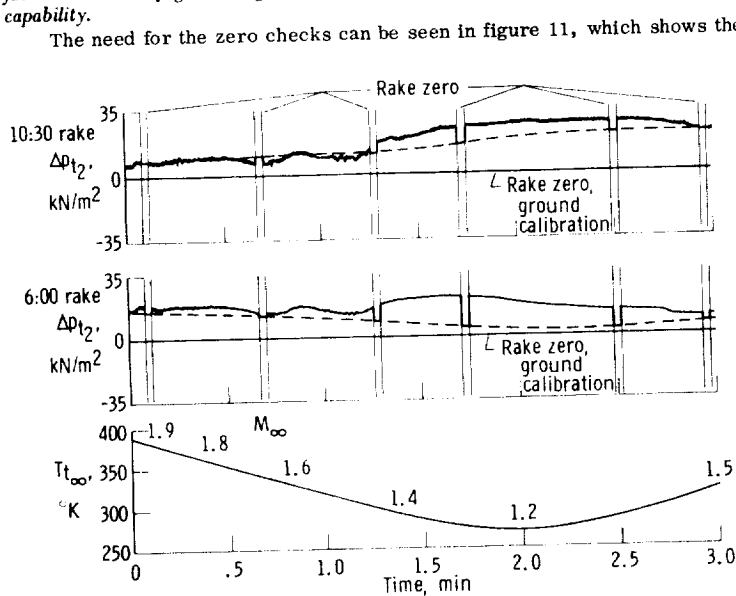Figure 10. Compressor face rake pressure zeros before and after a stall.

The need for the zero checks can be seen in figure 11, which shows the traces of 2 compressor face rake pressures over a 3-minute period of flight. During this period, the airplane decelerated from $M_\infty = 1.9$ to 1.2 and accelerated back to $M_\infty = 1.5$. Six rake zeros were taken during this time. The dashed line is faired through the zeros for each pressure. The in-flight zeros are well above the zero value that occurred on the ground calibration. Zeros for the 6:00 rake pressure shift back toward smaller errors with the decreasing temperature, but the 10:30 rake pressure zero increases with decreasing temperature. Also, the shifts are not consistent functions of temperature, but lag or lead unpredictably. These inconsistencies made it impossible to compensate for zero shifts by measuring the rake temperature near the transducer.

Figure 11. Time history of F-111A compressor face rake pressures showing zero shifts with temperature during supersonic flight.

Frequency response of the inlet pressures was determined, and results are shown in reference 1. The nulling compressor face rake acoustic response is flat to 400 hertz and usable, with reasonable corrections, to 1000 hertz.

Additional instrumentation, described in reference 6, was used to determine total temperature, engine airflow, airplane Mach number, altitude, angle of attack, inlet spike and cone position, and the value of the reference pressure supplied to the differential transducers.

DATA RECORDING

Output signals from the transducers were digitized by pulse code modulation (PCM) systems and recorded on magnetic tape. Two PCM systems were used, each with 77 channels sampled 200 times per second. The compressor face pressures were sampled 400 times per second by using two channels for each pressure, thus allowing frequency analysis to be extended from 100 hertz to 200 hertz. All compressor face pressure signals were filtered electrically prior to digitizing, to remove high frequencies, with cutoff starting at 200 hertz. Two of the compressor face pressures were also recorded on a wide-band frequency modulation (FM) system to permit analog analysis to much higher frequencies. These two channels were filtered, with cutoff starting at 1000 hertz, prior to recording.

Outputs of the PCM and FM systems were recorded on an onboard tape recorder. Part of the data was also telemetered to the ground to permit real time data monitoring and analysis.

DATA REDUCTION

Flight tapes containing the digital data were processed using a digital computer. Voltage monitor corrections and zero corrections were incorporated, and calibrations were applied. Output data were available in the form of parameter listings, calculated performance time histories, time history plots, and cross plots. The digital data were statistically analyzed by a digital computer program.

Analog pressure data and digital pressure data converted to analog data were processed by using a hybrid spectrum analyzer. In some instances, this system was used for real time analysis of pressures during flights.

DATA ANALYSIS

Several parameters are used in this paper to describe and analyze the pressure fluctuations observed in the inlets.

Instantaneous Parameters

A parameter which can be calculated with one sample of data from each pressure may be said to be "instantaneous,"

within the limitation of the sampling rate of 400 per second.

Pressure recovery.— The compressor face average total pressure recovery is calculated by averaging the probe values and dividing by the free-stream total pressure.

Distortion factor, K_D.— A distortion parameter derived by Pratt & Whitney for the TF30 engine is the K_D parameter. It considers the circumferential extent of distortion and weighs distortion near the engine hub more heavily than at the tip. The K_D parameter is defined as follows:

$$K_D = \frac{\sum\limits_{r=1}^{n}\left[\left(\frac{\Delta p}{p}\right)_r \left(\frac{d_o}{d_r}\right)_r \overline{\theta}_r\right]}{\sum\limits_{r=1}^{n}\left(\frac{d_o}{d_r}\right)}$$

where

r a particular ring of total pressure probes

$\left(\frac{\Delta p}{p}\right)_r = \frac{Pt_{av} - Pt_{min}}{Pt_{av}} \times 100$, in percent, for a particular ring

Pt_{av} average pressure per ring

Pt_{min} minimum pressure per ring

d_o outer diameter of duct

d_r diameter of a particular ring

$\overline{\theta}_r$ circumferential extent of largest single pressure depression below Pt_{av}, in degrees, for a particular ring (see adjacent sketch)

n number of measurement rings

Circumferential position, deg
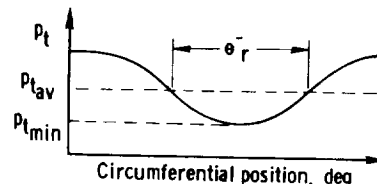
Statistical Parameters

Computation of statistical parameters such as those discussed below requires a considerable amount of data. These parameters are described briefly here; more rigorous definitions are presented in reference 8.

Turbulence factor, T_u.— The dynamic activity of a fluctuating pressure is indicated by the turbulence parameter, T_u, defined as the root mean square total pressure level divided by the average total pressure.

$$T_u = \frac{Pt_{rms}}{Pt_{2_{av}}}$$

Power spectral density, PSD.— A useful parameter for detecting predominant frequencies in a fluctuating pressure is the power spectral density parameter, PSD. It is also useful in comparing data from separate sources, such as flight data to wind-tunnel data or ground facility data. The square root of the area under the PSD curve is equal to the turbulence factor.

Coherence.— The coherence function provides a measure of the extent to which the pressure fluctuations at two probes arise in common sources, that is, the linear interdependence of the two pressures, at a specific frequency. Coherence ranges from 0 (no interdependence) to 1.0 (perfect interdependence). Coherence values less than 0.2 generally indicate no significant interdependence.

Phase angle.— The phase angle function provides an indication of the time delay between the two pressures as a function of frequency. For example, two pressures with a common frequency are 180° out of phase if at an instant of time one pressure is at a maximum while another pressure is at a minimum.

Calculation of statistical parameters.— The statistical parameters were calculated from the digital data by using a fast Fourier transform digital program. Input data were detrended prior to analysis to remove any very low frequencies. A total of 2048 data points (5.12 seconds) was used for the 400 samples per second compressor face pressure data, with an equivalent filter bandwidth of 2 cycles. A total of 1024 data points (5.12 seconds) was used for the cowl lip rake, shock position probe, duct total and static pressures, and engine pressures, all of which were sampled 200 times per second. The statistical parameters were valid for frequencies up to one-half of the sampling rate (ref. 8); however, some of the pressures were filtered to less than one-half of the sampling rate because of the probe resonant frequencies.

Power spectral densities calculated from the analog recording system were extended to 1000 hertz, even though the probe response was not flat beyond about 400 hertz. Eight seconds of data were used with an equivalent two-cycle bandwidth filter.

Duct Resonance Analysis

The formula for the resonant frequency of a pipe open at one end is given in reference 9 by

$$f_1 = \frac{c}{2(l + 0.82a)}$$

where

f_1 first fundamental frequency of the pipe

c speed of sound, m/sec

l pipe length, m

a average pipe radius, m

If the flow velocity in the pipe is not small, the following correction can be made:

$$f_1' = f_1(1 - M_{d_{av}}^2)$$

where

f_i' first fundamental frequency corrected for flow

$M_{d_{av}}$ average Mach number of the flow

The quantity $M_{d_{av}}$ was determined by calculating the Mach number at several duct stations using the known engine airflow and the duct area distribution, and averaging the results. Substituting for the speed of sound, this becomes

$$f_i' = 20.4 \frac{\sqrt{\dfrac{T_t}{1 + 0.2M_{d_{av}}^2}}}{2(l + 0.82a)} (1 - M_{d_{av}}^2)$$

For the F-111A inlet duct

$$l = 4m, \quad a = 0.4m$$

so

$$f_i' = 2.38 \sqrt{T_t} \frac{(1 - M_{d_{av}}^2)}{\sqrt{1 + 0.2M_{d_{av}}^2}}$$

For the engine fan duct resonance

$$l = 2.74m, \quad a = 0.3m$$

$$f_i' = 3.4 \sqrt{T_t} \frac{(1 - M_{d_{av}}^2)}{\sqrt{1 + 0.2M_{d_{av}}^2}}$$

RESULTS AND DISCUSSION

Steady-State Performance

The steady-state performance of the inlet is shown in terms of the inlet total pressure recovery and distortion factor, as a function of mass flow ratio and angle of attack, for a Mach number of about 2.15. Wind-tunnel data from a 1/6-scale model (ref. 10) are also shown for comparison. As shown in figure 12, the flight recovery data are relatively insensitive in the subcritical region to mass flow ratio and are slightly lower than the wind-tunnel results. The inlet becomes unstable at a mass flow ratio of about 0.80, as predicted by the wind-tunnel results. An inlet duct resonance discussed in a later section occurs between $m/m_0 = 0.89$ and 0.94.
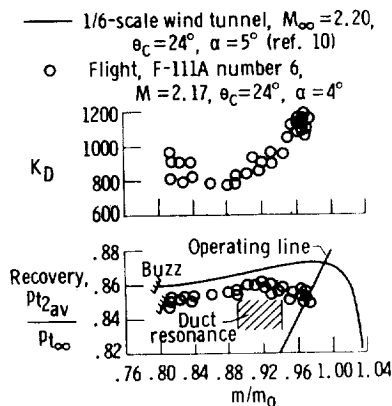
The operating point, m/m_0 of 0.97, is above the resonance mass flow and appears to represent slightly supercritical operation. The lower mass flow and recovery are probably due to fuselage boundary-layer ingestion which did not occur in the wind-tunnel tests. The K_D distortion factor increases rapidly with increasing mass flow ratio except for mass flow ratios near the stability limit. Values of K_D at the operating point are near the stall value, as will be discussed in the compressor stall section. Data obtained at a slightly lower Mach number are shown in figure 13 as a function of angle of attack. Both recovery and distortion increase as angle of attack increases from $2°$ to $6°$. Further increases in angle of attack have only a small effect on recovery and distortion. A single wind-tunnel data point at $\alpha = 5.5°$ agrees well with the flight data.

Using the manual inlet control system, the left inlet could be operated at off-schedule positions of the inlet spike and cone. Variations in inlet recovery, distortion, and turbulence factor as a function of inlet spike and cone position are reported in reference 6 for F-111A number 6. A typical example is shown in figure 14 at a Mach number of 1.60. Recovery, distortion factor, and turbulence factor are plotted as functions of spike position with the cone fixed and as functions of the cone angle with the spike fixed. The automatically scheduled positions are nearly optimum at this flight condition. Moving the spike aft has only a small effect, but moving the spike forward increases the turbulence factor and K_D and results in compressor stall. The cone can be fully retracted, but K_D and turbulence

Figure 12. Effect of mass flow ratio on inlet recovery and distortion.
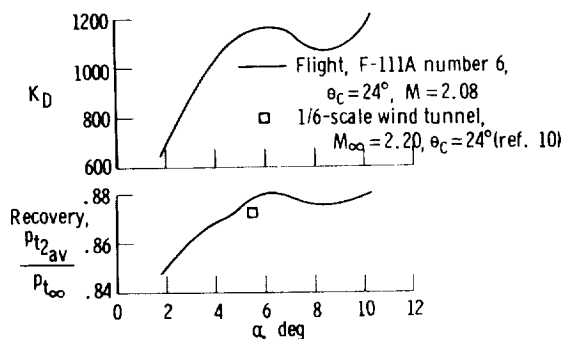

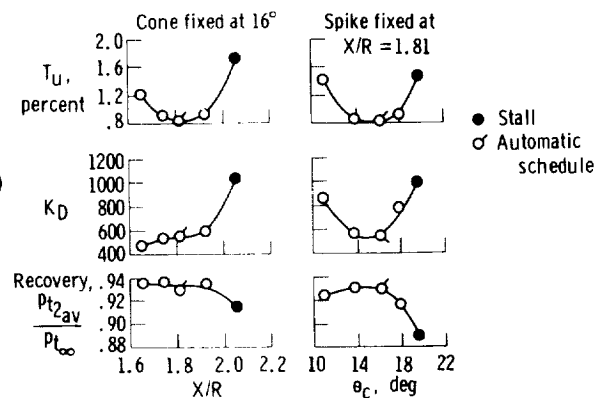*Figure 13. Effect of angle of attack on inlet recovery and distortion.*

Figure 14. Effect of spike and cone position on inlet performance at Mach 1.60.

rise to near the stall level. Expanding the cone decreases recovery and increases turbulence and distortion and causes a compressor stall.

Dynamic Analysis

Compressor stall analysis.— The occurrence of TF30 engine compressor stalls in the F-111A airplanes could not be satisfactorily correlated with inlet conditions until dynamic pressure measurements were made at the engine compressor face (ref. 4). Four of the eight compressor face rakes tested in F-111A number 6 were low response types and were used to obtain low response inlet recovery and distortion. A typical time history of the inlet distortion leading to compressor stall is shown in figure 15. At the time the stall was initiated, the low response distortion calculated at 50 samples per second was slowly decreasing with no indication of the approaching stall. The other four compressor face rakes, using the high response miniature transducers and picking up the high frequency pressure fluctuations, were used to calculate the same distortion factor at 400 samples per second. A peak occurs about 15 milliseconds prior to the stall. As explained in reference 4, 15 milliseconds is the time required for the distortion to reach the high pressure compressor stages in which the flow breakdown occurs and for the resulting hammershock to propagate back to the compressor face. The time interval agrees well with intervals obtained in ground facility tests of a TF30 engine at the NASA Lewis Research Center (ref. 11). The average levels of the two distortion factors are about the same, but the dynamic pressure fluctuations cause the high response K_D to vary by ±50 percent. The peak in the K_D that caused the stall lasted only a few milliseconds.
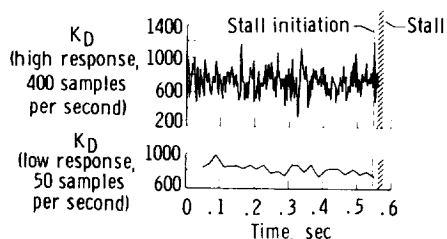

Figure 15. High and low response distortion factor for a compressor stall at Mach 1.60.

This peak in distortion factor 15 milliseconds prior to a compressor stall occurred in each of the 25 stalls analyzed from F-111A number 6. However, in some instances, this peak was not as high as other peaks during a previous data run. This was attributed mainly to the use of only four high response rakes. Reference 12 shows that five or more rakes are desirable. F-111A number 12 tests with eight high response rakes yielded more consistent distortion peaks prior to stall. Because of their in-flight nulling capability, the absolute level of each pressure, and, hence, the overall distortion factor levels were more accurate. Figure 16 compares the distortion factors for a stall using all eight rakes, only the diagonal rakes, and only the vertical and horizontal rakes for the same set of data. The eight rake K_D value at the time of stall initiation is higher than any previous peaks, but the K_D value calculated from the horizontal and vertical rakes is lower than many previous peaks and is therefore not a good indication of the stall. The diagonal rakes give almost as good an indication as all eight rakes because, in this instance, the lowest total pressure and the highest turbulence is in the region surveyed by the 7:30 rake.

Instantaneous total pressure maps were made from the F-111A number 12 40-probe data. A series of six maps taken in 23 milliseconds is shown in figure 17 for the compressor stall data of figure 16. The first two maps were taken prior to the stall initiation. Map 3 shows the high distortion that caused the stall with the K_D value of 1367. Maps 4 and 5 were taken while the stall was developing in the compressor, and in map 6 the high pressure hammershock wave appeared in the middle of the compressor face.
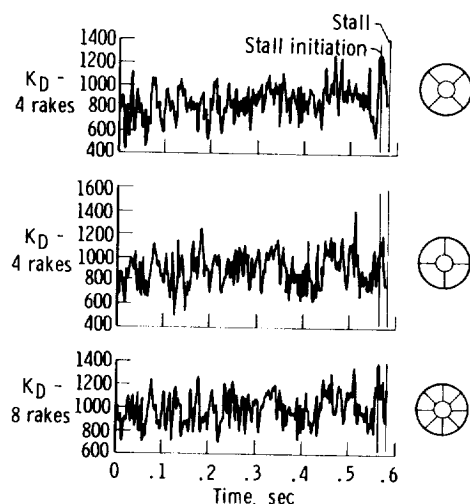

Figure 16. Effect of the number of rakes on the distortion factor, K_D, for a stall at $M_\infty = 2.0$.

Figure 17. Instantaneous compressor face maps for a stall at Mach 2.0. Numbers indicate total pressure recovery, percent.

A buildup in the distortion is evident in maps 1, 2, and 3 as the low pressure (dark) area moved toward the hub and enlarged and the high pressure area increased in size. The high distortion lasted only 3 milliseconds (about 1/2 rotor revolution) and in the next sample, map 4, the distortion was considerably lower. The appearance of the hammershock near the hub is consistent with the occurrence of the stall in the compressor stages and not in the fan.

Studies of the pressure fluctuations that occur in the inlet flow just prior to stall often reveal an out-of-phase relationship. This is shown in a "drift" type of stall (fig. 18), with the 1:30 rake pressures all rising and the 7:30 rake pressures all dropping at the same time. Although no particularly high or low pressure peaks occurred, the out-of-phase effect raised the distortion factor to a predominant peak and caused a compressor stall.
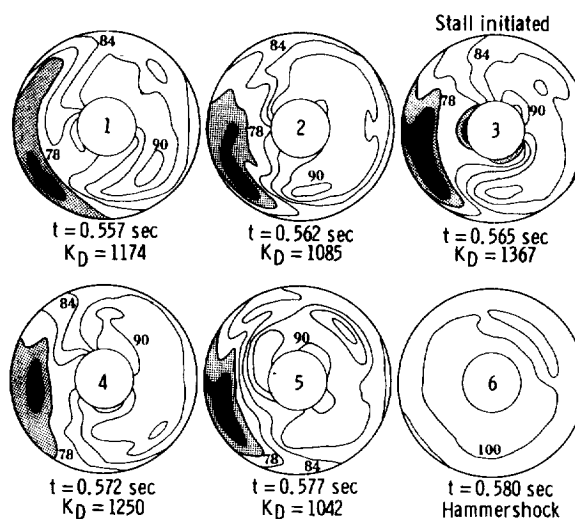
The K_D values at stall are summarized in figure 19 as a function of corrected engine airflow. Most of the data points are from F-111A number 6, but a few points from F-111A number 12 are shown and agree well with the F-111A number 6 data. Values of K_D at stall increase with corrected engine airflow. The sixth stage bleeds increase the K_D values at stall about 200. Stalls encountered without afterburning showed an additional K_D margin of about 150.
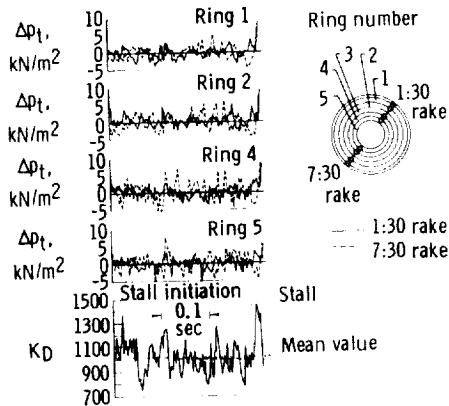

Figure 18. Pressure traces on opposite sides of the compressor face and distortion factor, K_D, for a stall at $M_\infty = 2.17$.

Figure 19. Summary of instantaneous distortion factor, K_D, values causing stall for F-111A number 6 and number 12. All data adjusted to Reynolds number index of 1.0.

In the previous discussion, only the distortion parameter, K_D, was presented; however, several other distortion parameters were also used. Some of these were discussed in reference 4. The Pratt & Whitney K_θ parameter and the Rolls Royce DC (θ) parameter have also been used for the F-111A number 12 data. Evaluation of these parameters is continuing.

The "instantaneous" distortion type of analysis is ideally suited to flight-test analysis of stalls, because only a few seconds of data leading up to the stall must be analyzed. In ground facility tests, many hours of test time are accumulated and it becomes prohibitively expensive to calculate instantaneous distortion factors for all the data. Reference 13 discusses statistical techniques for predicting the maximum distortion and relates it to the measured instantaneous distortion. Data from ground facility tests using actual engines may be analyzed by using the instantaneous distortion technique. Reference 14 presents results of wind-tunnel and altitude facility tests of a variety of engines, in addition to the flight data shown here.

Inlet duct resonance.— A resonant mode of the inlet duct has been observed in the inlet pressure data at certain flight conditions. The resonance was first detected in PSD plots of compressor face total pressures, for example, figure 20, which shows a PSD of four compressor face pressures from F-111A number 6 at $M = 2.0$. The resonant frequency of 27 hertz is evident on these probes, and a harmonic at 54 hertz can also be seen. Pressure traces for these same four probes are presented in figure 21. The 10:30 and 1:30 rakes have an obvious 27 hertz fluctuation. The 4:30 and 7:30 rake pressures show very little evidence of the resonance, and the power spectral densities of figure 20
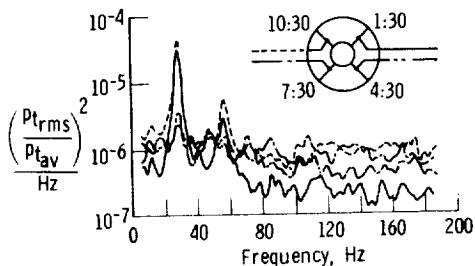

Figure 20. PSD's of four compressor face total pressures during duct resonance at $M_\infty = 2.0$.

Figure 21. Time history of compressor face total pressures during duct resonance at $M_\infty = 2.0$.

are required to detect its presence. Coherence plots showing the degree of interdependence between two pressures are presented in figure 22. The 10:30 rake pressure is compared to the 4:30, 7:30, and 1:30 rake pressures, and the coherence is highest for the 1:30 pressure. Phase angle plots between five pressures on the 1:30 and 10:30 rakes are shown in figure 23. At the 27 hertz resonance, phase angles of about $180°$ are seen, whereas at other frequencies, phase angles are random. This $180°$ phase angle can also be seen in figure 21 between the 1:30 and 10:30 rake pressure traces.

The magnitude of these fluctuations and the out-of-phase condition suggested that the compressor face distortion might be strongly affected by the resonance. The distortion factor was calculated for the data shown in the previous figures, and the 27 hertz fluctuation is obvious in figure 24. The peak K_D values are almost high enough to cause a compressor stall. An instantaneous map taken at the high K_D value shows a very high recovery region at the 1:30 rake and a very low recovery region at the 10:30 rake. This contrasts with the normal map at the lower K_D.

This duct resonance was usually observed at Mach numbers between 1.8 and 2.1. Its occurrence, strength, and frequency were found to be functions of the inlet geometry position, engine airflow, and free-stream Mach number. Intensity of the resonance was plotted qualitatively on a plot of spike position versus cone angle (fig. 25). A region of
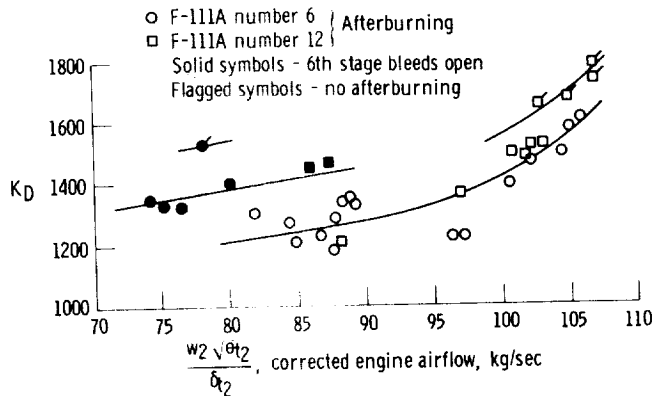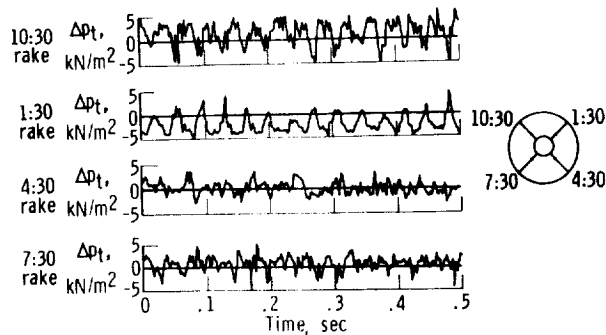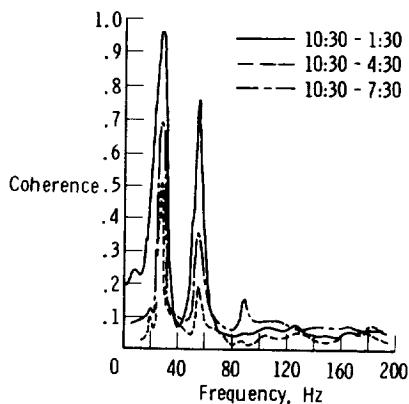
Figure 22. Coherence between 10:30 rake pressure and three other pressures during duct resonance at $M_\infty = 2.0$.
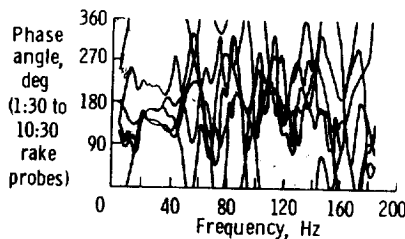

Figure 23. Phase angle between 1:30 rake and 10:30 rake pressures during duct resonance, $M_\infty = 2.0$.
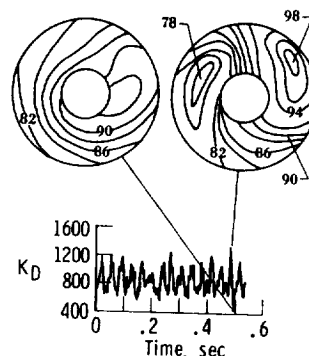

Figure 24. Distortion factor, K_D, and instantaneous compressor face maps during duct resonance at $M_\infty = 2.0$
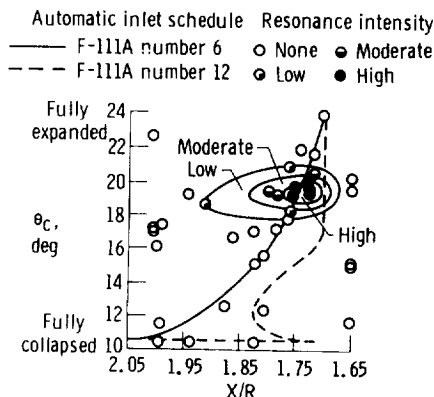

Figure 25. Effect of spike and cone position on the intensity of resonance.

the strongest resonance existed at a particular combination of spike and cone settings. The inlet control system automatically set the spike and cone in this region between Mach 1.9 and 2.05 on F-111A number 6 as indicated; however, with the manual inlet control system, the pilot could set the inlet geometry to off-schedule positions. The F-111A number 12 automatic schedule positioned the spike farther aft, and only weak resonance was encountered in the automatic mode. The spike position for strongest resonance places the inlet minimum area slightly inside the cowl lip (figs. 5 and 6) particularly with the blunt lip cowl, whereas the cone position results in an inlet throat Mach number of about 1.0. This situation might permit the inlet terminal shock wave to oscillate between the normal external position and an abnormal internal position.
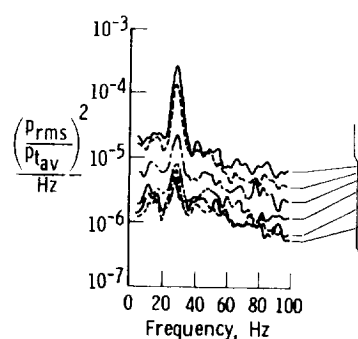
Power spectral density plots for the cowl lip rake total pressures, cowl lip rake static pressures, inlet duct total and static pressures, and shock position probe static pressures are presented in figures 26(a) to (d), respectively. These plots show evidence of the resonant frequency everywhere except on the cowl lip total pressures on the inboard side of the inlet. The resonance is extremely strong at the upper part of the inlet near the cone surface. A rake located in this area shows a
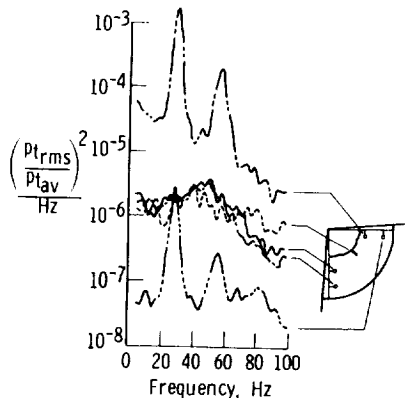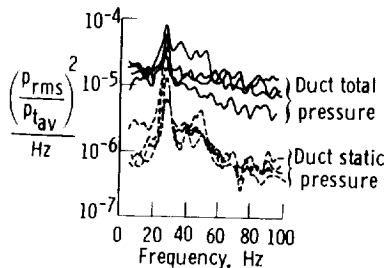

(a) Cowl lip total pressures.
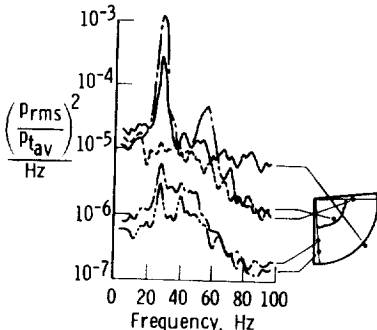
(b) Cowl lip static pressures.

(c) Shock position probe static pressures.

(d) Inlet duct total and static pressures.

Figure 26. Power spectral density plots of inlet pressures during duct resonance at $M_\infty = 2.0$.

predominant separation and reattachment cycle, as seen in figure 27, which shows the rake total pressure and the static pressure at the rake base. The distortion factor from figure 24 is repeated, and the direct effect can be easily seen at the compressor face with the slight delay due to the duct transport time. The highest K_D peaks follow the lowest inlet rake pressure levels.

These results suggest that the normal shock wave oscillation occurs as shown in figure 28. The shock wave is inside and nearly stable at the lower part of the inlet and jumps from the internal to the external position at the top. The shock wave moving forward separates the boundary layer on the cone, causing the extreme fluctuations seen in figure 27 near the cone surface. This separation generates additional oblique shock waves upstream of the normal shock, which momentarily result in high pressure recovery near the upper cowl lip. This combination of low energy separated flow inboard and high energy air outboard then flows down the duct and causes the low and high recovery areas seen at the compressor face in figure 24. As this is happening, the shock wave returns to the internal position. Numerous phase angle and coherence plots and studies of time histories that are not shown substantiate this explanation.
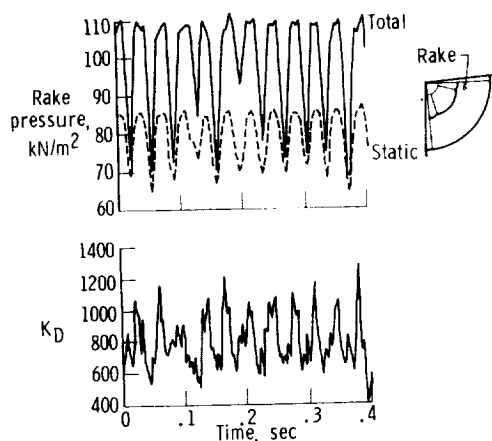
Figure 27. Comparison of inlet cowl lip rake total and static pressures with compressor face distortion factor, K_D, during duct resonance at $M_\infty = 2.0$.

Figure 28. Sketch of the inlet showing the normal shock wave in the external and internal position.

The precise frequency of this cycle is governed by the static pressure pulse generated by the movement of the normal shock wave. The duct acts as an open pipe and, at or slightly inside the compressor face, the wave is reflected back to initiate another shock movement. A simple formula for a pipe open at one end corrected for flow effects was described earlier and approximately predicts the observed resonance frequencies and their variation with engine airflow (duct Mach number) and free-stream Mach number (total temperature).
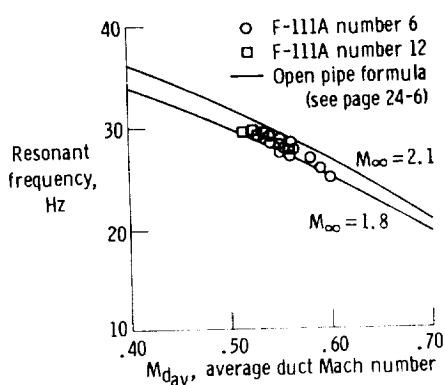

Figure 29. Comparison of measured resonant frequency to theoretical open pipe frequency. F-111A inlet duct; $M_\infty = 1.8$ to 2.1.

Figure 29 shows the frequency predicted by this formula as a function of the average duct Mach number for a total temperature representative of Mach numbers of about 1.8 to 2.1. Data points shown are the measured frequencies from F-111A number 6 and agree well with the calculated frequencies. Data from F-111A number 12 are also shown and are consistently higher in frequency and lower in average duct Mach number than those for the number 6 airplane because of the different duct area distribution (fig. 6).

The resonance disappears from digital power spectral densities at airplane Mach numbers below about 1.8, probably because the normal shock wave is stably positioned outside the duct. However, very weak resonant fluctuations can be seen in the analog power spectral densities in certain regions of the compressor face where random fluctuations are very small, at lower supersonic and even subsonic Mach numbers.

At Mach numbers between 2.1 and 2.3, the resonance is not seen except at reduced mass flow ratio (fig. 12). At the higher mass flow operating point, the normal shock appears to be inside the inlet (supercritical); and at lower mass flows (below 0.89 m/m_0), the shock is stable outside the inlet (subcritical operation). Only in the 0.89 to 0.94 m/m_0 range is the shock wave sufficiently unstable to sustain the resonance.

Rotor Speed Harmonics

Other discrete frequencies detected in the compressor face total pressures are the rotor speed frequencies and their harmonics. These frequencies are generated by shock waves from the blade tips operating at supersonic speeds and result in the multiple pure tone noise discussed in reference 15. The low pressure compressor frequency is typically 150 hertz and was detected in digital power spectral dens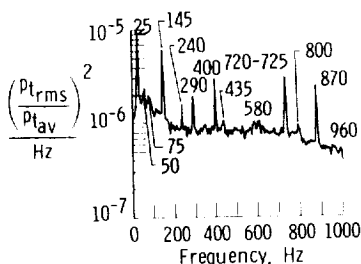ities. Analog power spectral densities of pressures filtered above 1000 hertz showed the 150 hertz peak and many more peaks due to the high pressure compressor rotor speed and harmonics of both rotor speeds. An example is shown in figure 30. The most predominant peaks in these data and in most other data are the fundamental and the fourth and fifth harmonics of the N_1 speed. Peaks at 400 and 800 hertz are due to the 400 hertz power supply frequency in the airplane. When the fan tip speed was subsonic, these frequencies were not evident.

Figure 30. Analog PSD of a compressor face total pressure showing various peaks due to duct resonance, rotor speeds, and power supply.

Source	Fundamental, Hz	Harmonics, Hz				
		1	2	3	4	5
Duct resonance	25	50	75	---		
Low rotor speed	145	290	435	540	725	870
High rotor speed	240	480	720	960	---	
Electrical power	400	800	---	---	---	

Fan Duct Resonance

A resonance detected in the fan duct and engine is believed to be due to a fan duct oscillation at a frequency of about 50 hertz. The instrumentation in the engine was not designed for high response; however, the sampling rate is sufficient for valid power spectral densities to 100 hertz. Probe resonance and data filtering make amplitude response uncertain above 40 hertz, but the predominant 50 hertz resonance is believed to be valid. Power spectral densities showing the eight fan duct total pressures and the low and high pressure compressor discharge static pressures are shown in figure 31. Figure 31(a) shows data for a Mach number of 2.04 with partial afterburning of the left engine. The spike at 50 hertz is evident in all the pressures. Figure 31(b) shows power spectral densities for the
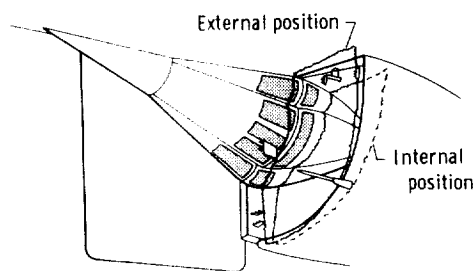
same pressures at $M_\infty = 2.08$ with the afterburner not lit, and there is a complete absence of any predominant frequencies up to the maximum value of 100 hertz. A third PSD is shown in figure 31(c) at $M_\infty = 2.15$ with maximum afterburning. It shows a definite resonance at 50 hertz, but the resonance is not on all probes and is of much less magnitude than that for the partial afterburning condition in figure 31(a).

(a) Partial afterburning, $M_\infty = 2.04$.　　(b) Nonafterburning, $M_\infty = 2.08$.　　(c) Maximum afterburning, $M_\infty = 2.15$.
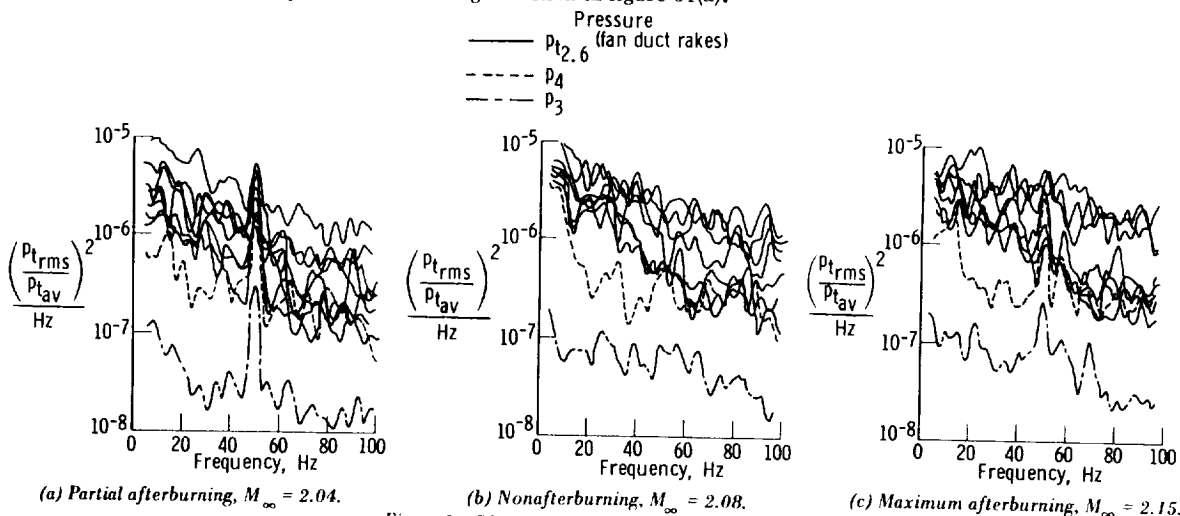
Figure 31. PSD of fan duct and engine pressures.

The fact that the resonance appears in the low and high pressure compressor as well as in the fan duct indicates that the pressure fluctuation is propagating through the fan stages into the compressor. This may explain the observed decrease in engine compressor stall margin with the afterburner lit, shown in figure 19. The relationship between the fan duct resonance and the afterburner operation suggests that a combustion instability is involved. The afterburning flame front may oscillate and generate pressure pulses which propagate back up the fan duct and reflect off the fan stages.

Although there are many modes of combustion instability, the most common is probably the longitudinal mode. Using the distance from the fan discharge to the afterburner flameholder, and a fan duct Mach number of 0.4, the same organ pipe equation used in the inlet duct estimates a fan duct frequency of 53 hertz, which is sufficiently close to the observed frequency of 50 to suggest that it may be the mode causing the fluctuation. Phase angles between the 10:00 and 2:00 fan duct pressures at 50 hertz are near $0°$ which also suggests a longitudinal mode. Reference 16 discusses afterburner instabilities and analytical techniques for predicting the frequencies and amplitudes.

FUTURE PROGRAMS

To acquire the depth of understanding necessary to apply generally the information obtained on the nature of inlet dynamics to future aircraft, several different types of inlets need to be studied. The F-111A tests are now complete, and preparations are being made to conduct a comparable program on a YF-12 airplane. This airplane (fig. 32) will permit the study of an axisymmetric, mixed compression type of inlet. Such an inlet presents new problem areas not encountered with the external compression F-111A inlets. Included are inlet unstarts and the effect of bypass flows on airplane aerodynamics. The large unsymmetrical drag resulting from one inlet unstarting while at cruise speeds near Mach 3 can cause severe handling problems and possibly complete loss of control.

Figure 32. Photograph of the YF-12 airplane.

Like most mixed or internal compression inlets the YF-12 inlet requires air to be bypassed ahead of the compressor at some speed and power conditions in order to maintain the terminal shock at the proper position. Preliminary flight studies in which tufts were photographed with a motion picture camera mounted in the fuselage showed that the bleed and bypass flows from the nacelle caused a large separated area in the wing-nacelle juncture region and pulsating flow along the surface of the nacelle. These flow effects are illustrated in figure 33, which was taken from reference 7. One-twelfth-scale model tests in a wind tunnel at the Ames Research Center showed that bypassing 37 percent of the intake air, a realistic value for some flight conditions, causes an increase in the overall airplane drag by an amount nearly equal to the zero-lift drag.

A schematic view of the inlet showing the location of the various sensors is shown in figure 34. Measurements at the tip of the centerbody will indicate the total pressure and direction of the airstream reaching the inlet. Static pressure orifices will show the location of the terminal shock, even when the inlet is unstarted, and enough of these sensors will be of the high response type that shock oscillations can be measured. There will be three internal boundary-layer rakes, one close to the throat and two farther downstream. These boundary-layer probes will be connected to dynamic pressure transducers so that rapid variation and oscillations of the boundary-layer pressures can be measured. Altogether, 50 to 70 dynamic pressure measurements will be made in the inlet.

Bleed and bypass flows will also be measured in flight. To make such measurements without an excessive amount of instrumentation, tests will be run on a full-scale inlet in the 10- by 10-foot wind tunnel at the NASA Lewis Research Center to define and calibrate the duct flow probes. The wind-tunnel tests will also give an indication of leakage flow through various joints and cracks. Sealing small cracks is extremely difficult because of the temperatures encountered by the inlet, and the leakage flow is believed to be significant.

The flight-measured performance of the YF-12 inlet will be correlated with data from the full-scale inlet in the Lewis 10- by 10-foot wind tunnel and with data on 1/3-scale and 1/12-scale models tested at the NASA Ames Research Center. Thus it should be possible to get an indication whether differences are due to scale effects or to basic

24-12

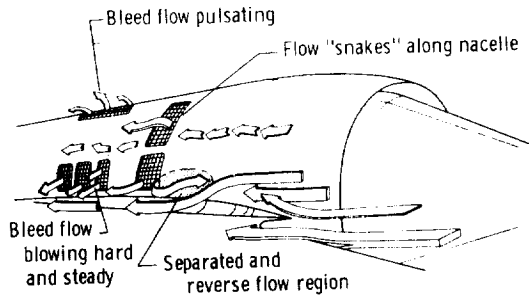differences between wind-tunnel and flight testing.

Figure 33. Flow patterns on nacelle of YF-12 airplane as determined from tuft studies. Mach 1.5, forward bypass open.
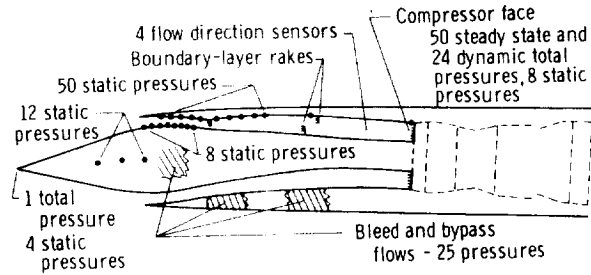
Figure 34. Instrumentation for YF-12 tests.

CONCLUDING REMARKS

The steady-state and dynamic pressure phenomena in the inlets of two F-111A airplanes were investigated. A new pressure survey rake incorporating miniature transducers and a slide valve to permit in-flight zero checks was used at the compressor face and was found to yield excellent steady-state and dynamic pressure data. Analysis of the high response pressure data showed the cause of compressor stalls to be high levels of instantaneous distortion lasting for times as short as 3 milliseconds. In many instances, the distortion causing the stall was due to an out-of-phase situation in total pressures on opposite sides of the compressor face. An inlet duct resonance at Mach numbers above 1.8 was analyzed by using time history and statistical parameters and was found to result from a normal shock oscillation at the duct fundamental frequency. Another resonance in the fan duct of the engine during afterburning operation may have affected the compressor stall margin. Plans for studies of the inlets of the YF-12 interceptor include flight tests and comparison with full-scale, 1/3-scale and 1/12-scale wind-tunnel tests.

REFERENCES

1. Smith, Ronald H.; Bellman, Donald R.; and Hughes, Donald L.: Preliminary Flight Investigation of Dynamic Phenomena Within Air Breathing Propulsion Systems of Supersonic Aircraft. AIAA Paper No. 68-593, 1968.
2. Martin, Richard A.: Dynamic Analysis of XB-70-1 Inlet Pressure Fluctuations During Takeoff and Prior to a Compressor Stall at Mach 2.5. NASA TN D-5826, 1970.
3. Bellman, Donald R.; and Hughes, Donald L.: The Flight Investigation of Pressure Phenomena in the Air Intake of an F-111A Airplane. AIAA Paper No. 69-488, 1969.
4. Burcham, Frank W., Jr.; and Hughes, Donald L.: Analysis of In-Flight Pressure Fluctuations Leading to Engine Compressor Surge in an F-111A Airplane for Mach Numbers to 2.17. AIAA Paper No. 70-624, 1970.
5. Burcham, Frank W., Jr.: An Investigation of Two Variations of the Gas Generator Method to Calculate the Thrust of the Afterburning Turbofan Engine Installed in an F-111A Airplane. NASA TN D-6297, 1971.
6. Martin, Richard A.; and Hughes, Donald L.: Comparisons of In-Flight F-111A Inlet Performance for On- and Off-Scheduled Geometry at Mach Numbers of 0.68 to 2.18. NASA TN D-6490, 1971.
7. Bellman, Donald R.; Burcham, Frank W., Jr.; and Taillon, Norman V.: Techniques for the Evaluation of Air-Breathing Propulsion Systems in Full-Scale Flight. NASA paper presented at AGARD 38th Flight Mechanics Panel Meeting, Toulouse, France, May 10-13, 1971.
8. Bendat, Julius S.; and Piersol, Allan G.: Measurement and Analysis of Random Data. John Wiley & Sons, Inc., c.1966.
9. Kinsler, Lawrence E.; and Frey, Austin R.: Fundamentals of Acoustics. Second ed., John Wiley & Sons, Inc., 1962, p. 201.
10. Hartin, J. P.: Wind Tunnel Investigation at Transonic and Supersonic Mach Numbers of Duct Modifications to the F-111A Inlet. AEDC-TR-66-19, Arnold Eng. Dev. Center, Feb. 1966.
11. Braithwaite, Willis M.; and Vollmar, William R.: Performance and Stall Limits of a YTF30-P-1 Turbofan Engine With Uniform Inlet Flow. NASA TM X-1803, 1969.
12. Oates, Gordon C.; Sherman, Dale A.; and Motycka, David L.: Experimental Study of Inlet-Generated Pressure Fluctuations. Tech. Rep. AFAPL-TR-69-103, Air Force Aero Propulsion Lab., Wright-Patterson Air Force Base, June 1970, pp. 427-457.
13. Kimzey, William F.; and McIlveen, Milton W.: Analysis and Synthesis of Distorted and Unsteady Turbo Engine Inlet Flowfields. AIAA Paper No. 71-668, June 1971.
14. Anon.: Aircraft Propulsion. NASA SP-259, 1971, pp. 283-349.
15. Pickett, Gordon F.: The Prediction of the Spectral Content of Combination Tone Noise. AIAA Paper No. 71-730, June 1971.
16. Dix, Donald M.; and Smith, George E.: Analysis of Combustion Instability in Aircraft Engine Augmenters. AIAA Paper No. 71-700, 1971.
17. Johnson, Clarence L.: Some Development Aspects of the YF-12A Interceptor Aircraft. AIAA Paper No. 69-757, 1969.